Carcinogenesis vol.32 no.1 pp.2–9, 2011
doi:10.1093/carcin/bgq209
Advance Access publication October 15, 2010

Pathologically decreased miR-26a antagonizes apoptosis and facilitates carcinogenesis by targeting MTDH and EZH2 in breast cancer

Bo Zhang[1,†], Xiao-Xiao Liu[2,†], Jian-Rong He[3], Ci-Xiang Zhou[1], Meng Guo[1,4], Ming He[1], Mei-Fang Li[3], Guo-Qiang Chen[1,2,4] and Qian Zhao[1,*]

[1]Department of Pathophysiology, Key Laboratory of Cell Differentiation and Apoptosis of National Ministry of Education, Ruijin Hospital, Shanghai Jiao-Tong University School of Medicine (SJTU-SM), Shanghai 200025, China, [2]Institute of Health Sciences, Shanghai Jiao-Tong University School of Medicine (SJTU-SM) & Shanghai Institutes for Biological Sciences (SIBS), Chinese Academy of Sciences (CAS), Shanghai 200025, China, [3]Department of General Surgery, Ruijin Hospital, Shanghai Jiao-Tong University School of Medicine, Shanghai 200025, China and [4]State Key Laboratory for Oncogenes and Related Genes, Shanghai Jiao-Tong University School of Medicine, Shanghai 200032, China

[*]To whom correspondence should be addressed. Department of Pathophysiology, Shanghai Jiao-Tong University School of Medicine, No. 280, Chong-Qing South Road, Shanghai 200025, China. Tel: +86 21 64666992; Fax: +86 21 64154900;
Email: qzhao@shsmu.edu.cn
Correspondence may also be addressed to Guo-Qiang Chen.
Tel/Fax: +86 21 64154900;
Email: chengq@shsmu.edu.cn

The role of miR-26a in carcinogenesis appears to be a complicated one, in the sense that both oncogenic and tumor suppressive effects were reported in cancers such as glioblastoma and hepatocellular carcinoma, respectively. Here, we report for the first time that miR-26a is downregulated in breast cancer specimens and cell lines and its transient transfection initiates apoptosis of breast cancer cell line MCF7 cells. Furthermore, retrovirus-delivered miR-26a impairs the *in vitro* colony forming and *in vivo* tumor-loading ability of MCF7 cells. Subsequently, MTDH and EZH2 are identified as two direct targets of miR-26a and they are significantly upregulated in breast cancer. MCF7 xenografts with exogenous miR-26a show that a decrease in expression of both MTDH and EZH2 is accompanied by an increase in apoptosis. Moreover, knockdown of MTDH causes apoptosis while reexpression of MTDH partially reverses the proapoptotic effect of miR-26a in MCF7 cells. Our findings suggest that miR-26a functionally antagonizes human breast carcinogenesis by targeting MTDH and EZH2.

Introduction

MicroRNAs represent a large family of endogenous noncoding RNAs and posttranscriptionally regulate gene expression (1). MicroRNAs are involved in tumorigenesis and function as oncogenes or tumor suppressor genes (2). It has been reported that 52.5% of microRNA genes are located in cancer-associated fragile sites (3). A large amount of microarray profile data shows miR-26a dysregulation in diverse cancers (4,5). The function of miR-26a has been investigated in several distinct cancers (6–8). In breast cancer, 72.8% of microRNA loci display alteration of DNA copy number (9); particularly, loss of heterozygosity is frequently seen at chromosome 3p22 where miR-26a is located (10,11).

Abbreviations: FBS, fetal bovine serum; NC, negative control; PCR, polymerase chain reaction; RT, reverse transcription; TUNEL, terminal deoxynucleotidyl transferase-mediated deoxyuridine triphosphate nick end-labeling; UTR, untranslated region.

[†]These authors contributed equally to this work.

Generally, dysregulated miR-26a exerts contrary functions in distinct cancers. When implicated as an oncogene, miR-26a greatly facilitates glioblastoma formation *in vivo* as an antagonist of phosphatase and tensin homolog (6,12), mitogen-activated protein kinase kinase kinase 2 and retinoblastoma 1 (6). On the contrary, miR-26a protects normal liver tissue from hepatocellular carcinoma-promoting inflammation (13) and successfully achieved the therapy of MYC-induced liver cancer via adeno-associated virus delivery, with attenuated expression of cyclin D2 (CCND2) and cyclin E2 (CCNE2) (7). Moreover, miR-26a is downregulated and appears to have broad antitumorigenic properties in both rhabdomyosarcoma and MYC-induced lymphoma (8,14). In breast tumor cell lines, miR-26a is subjected to downregulation following 17β-estradiol treatment in an estrogen receptor-dependent manner and is predicted to be associated with cell proliferation (15). Therefore, functional studies of miR-26a could shed light on the pathological mechanisms of breast cancer.

Since microRNAs are universally reduced in different tumors (16), we paid attention to high-expression genes computationally predicted as putative miR-26a targets in human breast carcinomas. Metadherin (MTDH) and enhancer of zeste homolog 2 (EZH2) are upregulated as high as 2.646- and 10.114-fold in breast cancer, respectively (17). MTDH facilitates malignant transformation of normal immortal cloned rat embryo fibroblast cells (18), whereas EZH2 promotes anchorage-independent growth and invasion of immortalized human mammary epithelial cells (19). Retrospective studies from clinical breast cancer patients indicate that high expression of MTDH or EZH2 is associated with short survival (19,20). MTDH promotes tumor proliferation and chemoresistance by activating the nuclear factor-kappaB signaling pathway (21–23), while also contributing to Ha-RAS- or c-MYC-mediated tumorigenesis by acting as one of their downstream targets (24). EZH2 turns out to be a bona fide oncogene and acts as a globally dual function transcription regulator (25) by converging on the methyltransferase activity silencing tumor suppressor genes, which are implicated in neoplastic development and the transactivation property-activating genes involved in the late-stage process of cancer (26,27). It has been reported that EZH2 protects kidney cancer cells from apoptotic stimulation (28).

In this study, we report that miR-26a is pathologically downregulated in breast cancer. Overexpression of miR-26a initiates breast tumor cell apoptosis by targeting MTDH and EZH2. Furthermore, miR-26a endows MCF7 cells with the ability to suppress anchorage-independent growth *in vitro* and tumorigenesis *in vivo*. Our findings indicate that manipulation of miR-26a as a clinically viable anticancer agent represents a promising therapeutic approach for breast cancer.

Materials and methods

Tissue specimens and cell lines

Human breast cancer specimens were collected from patients undergoing surgical resection in the Department of General Surgery, Ruijin Hospital, Shanghai Jiao-Tong University School of Medicine. Fresh breast carcinomas and paired adjacent normal tissues were immediately snap-frozen in liquid nitrogen and preserved in −80°C until use and their histological type was further confirmed using standard hematoxylin and eosin staining. This study was approved by the Research Ethnics Committee of Shanghai Jiao Tong University School of Medicine. Informed consent was obtained from all patients.

CCD-1095Sk, an immortalized human normal breast skin cell line, was maintained in Dulbecco's modified Eagle's medium (Hyclone, Logan, UT) supplemented with 10% fetal bovine serum (FBS; Gibco BRL, Gaithersburg, MD), 0.1 mM non-essential amino acids (Hyclone, Logan, UT), 1.0 mM sodium pyruvate (Hyclone, Logan, UT) and 100 U of penicillin–streptomycin. Human breast cancer cell lines MCF7 and an immortalized human embryonic kidney cell line HEK293 were cultured in Dulbecco's modified Eagle's medium with 10% FBS. Human breast cancer cell lines MDA-MB-231 and

© The Author 2010. Published by Oxford University Press. All rights reserved. For Permissions, please email: journals.permissions@oup.com

Downloaded from https://academic.oup.com/carcin/article/32/1/2/2477079 by U.S. Department of Justice user on 17 August 2022

MDA-MB-468 were cultured in Leibovitz L-15 medium (Gibco BRL, Gaithersburg, MD) with 10% FBS. Human breast cancer cell lines HCC1937, BT-549 and BT-474 were cultured in RPMI 1640 (Hyclone, Logan, UT) with 10% FBS. All cells were grown in a humidified atmosphere of 5% CO_2 and 95% air, except for MDA-MB-231 and MDA-MB-468, which were grown in 100% air at 37°C.

RNA extraction and stem-loop reverse transcription–polymerase chain reaction

Total RNA was extracted using Trizol reagent (Invitrogen, Paisley, Scotland, UK) following the supplier's procedure with slight modifications. After lysed with 1 ml Trizol reagent, the cells or tissues were incubated for 5 min at room temperature. The lysates and 300 µl chloroform were vigorously mixed and laid for 15 min at room temperature. After centrifugation for 20 min at 4°C, 500 µl isopropanol was applied to precipitate RNA in the upper solution following centrifugation. Subsequently, RNA was dried and dissolved with RNase-free water.

To determine the abundance of miR-26a, we employed a polymerase chain reaction (PCR)-based quantification technique called quantitative stem-loop reverse transcription (RT)–PCR (29). After removal of DNA contamination using RQ1 RNase-free DNase (Promega, Madison, WI), 1250 ng total RNA was utilized for RT with ImProm-II™ Reverse Transcription System (Promega, Madison, WI). According to the method reported by Chen *et al.* (29), mature miR-26a and U6 snRNA were reversely transcribed using Stem-loop RT primer miR-26a-RT (supplementary Table S1 is available at *Carcinogenesis* Online) and random primers of non-adeoxyribonucleotide mixture (TaKaRa, Dalian, China), respectively. Real-time PCR was performed using SYBR Green PCR Master Mix (Applied Biosystems,Warrington, UK) in an Applied Biosystems 7300 instrument. The primer pairs for miR-26a and U6 amplicons are miR-26a-F/R and U6-F/R (supplementary Table S1 is available at *Carcinogenesis* Online), respectively. Expression data were uniformly normalized to the internal control U6 and the relative expression levels were evaluated using the $2^{-\Delta\Delta Ct}$ method.

RNA oligoribonucleotide

Both negative control (NC) and miR-26a mimics were composed of RNA duplexes (GenePharma,Shanghai,China) with the following sequence orientated from 5′ to 3′, miR-26a: UUCAAG-UAAUCCAGGAUAGGCU/CCUAUCCUGGAUUACUUGAAUU and NC: UUCUCCG-AACGUGUCACGUTT/ACGUGACACGUUCGGAGAATT. The small interference RNAs siMTDH and siEZH2 are double-strand RNAs consisted of the following sequence orientated from 5′ to 3′, siMTDH: GGAGGAGGCUGGAAUGAAAdTdT/dTdT-CCUCCUCCGACCUUACUUU and siEZH2: GAGGUUCAGACGAGCUGAUdTdT/dT-dTCUCCAAGUCUGCUCGACUA (RiboBio, Guangzhou, China). Neither control microRNA mimics nor control small interference RNAs shares any homologous region with the human genome sequences.

Detection of cell viability

A total of 3.5×10^3 MCF7 cells with 100 nM microRNA mimics or small interference RNA oligonucleotides and 0.375 µl Lipofectamine 2000 (Invitrogen, Paisley, Scotland, UK) were inoculated in each well of 96-well plates. Fresh complete medium was changed for cells at 24 h post-transfection except for those cells to be tested for viability at this time point. To determine whether miR-26a-mediated cell viability reduction was ascribable to its targets, MCF7 cells were transfected with 100 ng of either pcDNA3.1-MTDH or pcDNA3.1 using 2.4 µl FuGENE 6 (Roche, Basel, Switzerland) at 24 h after NC or miR-26a mimics transfection in 96-well plates. Ten microliters of Cell Counting Kit-8 (Dojindo, Kumamoto, Japan) was added to each well and then incubated for 2 h at 37°C. The optical density at 450 nm was detected using a microplate reader. Cell Counting Kit-8 assays were performed at 24, 48, 72 and 96 h after transfection.

Apoptosis assay

DNA fragmentation from the apoptotic cells was assessed through a terminal deoxynucleotidyl transferase-mediated deoxyuridine triphosphate nick end-labeling (TUNEL) assay using an *in situ* cell death detection kit (Roche, Basel, Switzerland). Briefly, 1.4×10^5 MCF7 cells with 250 pmol NC or miR-26a mimics were inoculated onto a sterile coverslip in each well of six-well plates. To evaluate whether miR-26a imposing traits in MCF7 cells were attributable to its targets, MCF7 cells were transfected with 0.25 µg of either pcDNA3.1-MTDH or pcDNA3.1 per well using 0.5 µl Lipofectamine 2000 at 24 h after NC or miR-26a mimics transfection in 24-well plates. At 24, 48, 72 and 96 h, the cells on the coverslip were fixed in 4% paraformaldehyde at room temperature for 1 h and then permeablized with cold methanol for 10 min. Following incubation with terminal deoxynucleotidyl transferase and fluorescein-labeled deoxyuridine triphosphate at 37°C for 1 h. The cells were counterstained with 4,6-diamidino-2-phenylindole (Dako, Denmark) and then visualized by fluorescence microscopy (Leica, Solms, Germany). We separately counted TUNEL-positive cells and total cells as determined by nuclear staining of each well and their ratio was considered as the percentage of TUNEL-positive cells. Following an analogous approach, cancer cell apoptosis of MCF7 xenografts was assessed in frozen sections.

The characteristic change of externalized phosphatidylserine residues in the apoptotic cells was evaluated by the double-staining method of fluorescein isothiocyanate-labeled annexin V and propidium iodide (BD Biosciences Pharmingen, San Diego, CA). MCF7 cells together with NC or miR-26a mimics and Lipofectamine 2000 were plated in each well of 12-well plates at an initial density of 1.0×10^5 cells. We harvested both attached and detached cells at 48,

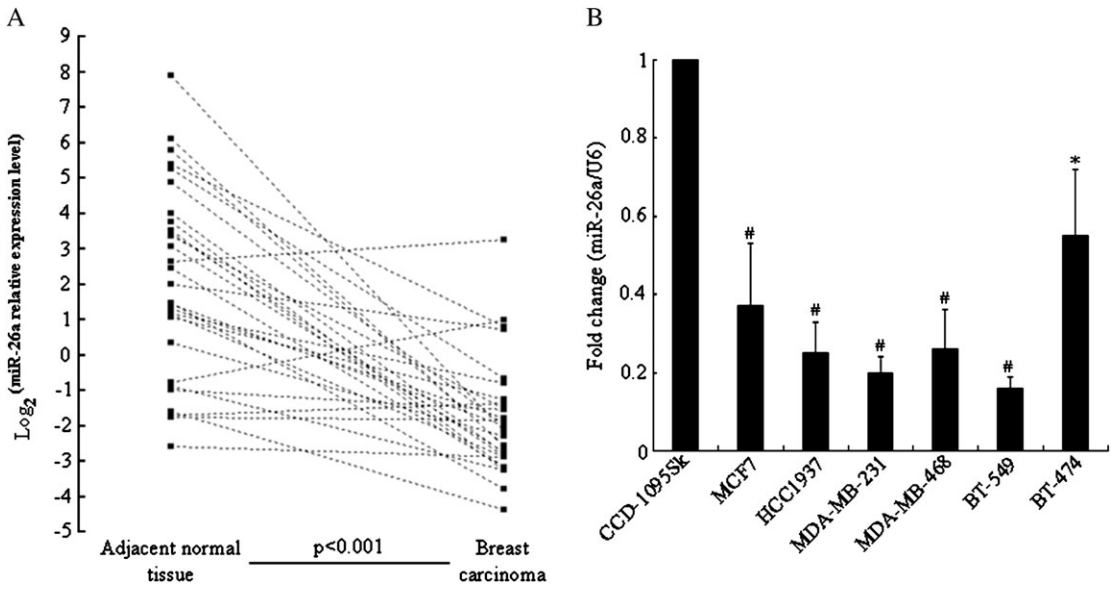

Fig. 1. Expression of miR-26a in human breast cancer tissues and cell lines. (**A**) Comparison of the expression level of miR-26a in 29 paired clinical cases. The dots represent the relative expression level of miR-26a normalized to the internal control U6 and each pair of dots connected by a dash line denotes a set of paired specimens. The miR-26a expression level of tumor and paired noncancerous tissues is collectively displayed in the right and left parts, respectively. (**B**) Difference of miR-26a expression in CCD-1095Sk and six breast cancer cell lines, MCF7, HCC1937, MDA-MB-231, MDA-MB-468, BT-549 and BT-474. The data in the vertical axis mean that the fold change of miR-26a expression in tumor cells relative to that of CCD-1095Sk. The symbols * and # denote significant statistical differences of $P < 0.05$ and $P < 0.01$, respectively, using a two-tailed Student's *t*-test.

Downloaded from https://academic.oup.com/carcin/article/32/1/2/2477079 by U.S. Department of Justice user on 17 August 2022

72 and 96 h and only the attached cells at 24 h due to the cytotoxicity effect of Lipofectamine 2000 by trypsinization and centrifugation. After resuspending with 1× binding buffer, a total of 1.0×10^5 cells were incubated with 5 μl annexin V for 15 min and then with propidium iodide for another 5 min at room temperature. Subsequently, the labeled cells were detected using flow cytometry (FACSCalibur; BD Immunocytometry Systems, San Jose, CA) and both early and late apoptotic cells were calculated by CellQuest software (FACSCalibur; BD Immunocytometry Systems, San Jose, CA).

In silico targets prediction of miR-26a

To explore miR-26a targets, we employed three online softwares, TargetScanS (http://genes.mit.edu/tscan/targetscanS2005.html), PicTar (http://pictar.org/) and miRanda (http://www.microrna.org/microrna) for computer-guided targets recognition. The outputs of the three distinct algorithms were processed to develop an overlap subset. Meanwhile, global analysis of gene expression from 47 human breast cancer cases was utilized to identify dysregulated genes (17). Consequently, miR-26a targets upregulated in breast carcinomas were acquired and further subjected to ranking as implemented in the miRanda algorithm based on alignment scores.

Luciferase assays

HEK293 cells were seeded in 24-well plates at a density of 2.0×10^5 cells per well and allowed to grow for 24 h before transfection. Then, each well was transiently cotransfected with 100 ng reporter plasmids of either wild-type or mutant 3′-untranslated region (UTR) construct pMIR-REPORT (Ambion, Austin, TX), 60 pmol NC or miR-26a mimics and 10 ng internal control vector pRL-SV40 (Promega, Madison, WI) using 1.44 μl Lipofectamine 2000. Cell lysates were harvested 24 h post transfection and then firefly and renilla luciferase activities were measured by the Dual-Luciferase Reporter Assay System (Promega, Madison, WI) on a Berthold AutoLumat LB9507 rack luminometer. The value of relative luciferase activity denotes the firefly luciferase activity normalized to that of renilla for each assay.

Plasmids

To stably express miR-26a in MCF7 cells, the retrovirus vector MSCVpuro-miR-26a was constructed. The 418 bp genomic segment encompassing the mature miR-26a-1 sequence and its 168 bp 5′ and 228 bp 3′ flanking regions were amplified using primers miR-26a-1-F/R (supplementary Table S1 is available at *Carcinogenesis* Online) and subcloned into BglII and EcoRI sites of the MSCVpuro vector. MCF7 cells were positively selected using puromycin (Sigma, St. Louis, MO).

For providing a direct proof that microRNAs can regulate the computationally predicted targets, the luciferase reporter vectors pMIR-REPORT with both wild-type or mutated 3′-UTR of potential targets were developed. The wild-type 1412 bp truncated 3′-UTR of MTDH (2112–3523 nt, GenBank accession no. NM_178812) and 278 bp full-length 3′-UTR of EZH2 (2286–2563 nt, GenBank accession no. NM_152998), both of which contain the putative miR-26a-binding sites, were amplified from the genomic DNA of MCF7 cells using primer pairs MTDH-UTR-F/R and EZH2-UTR-F/R (supplementary Table S1 is available at *Carcinogenesis* Online), respectively. The two amplicons were directionally cloned into the immediate downstream of the luciferase gene in the reporter plasmid pMIR-REPORT by MluI and HindIII. The site-directed mutagenesis kit (Stratagene, La Jolla, CA) was utilized to introduce four mutated bases into the predicted miR-26a-binding sites for 3′-UTRs of MTDH and EZH2 using the primer pairs MTDH-Mut-F/R and EZH2-Mut-F/R (supplementary Table S1 is available at *Carcinogenesis* Online), respectively.

To construct MTDH expressing vector, a 1814 bp fragment was amplified with MTDH-F/R primer pairs (supplementary Table S1 is available at *Carcinogenesis* Online) from the complementary DNA of MCF7 cells. Using semi-nested PCR approach, 1749 bp coding region was amplified with MTDH-NF/R primers (supplementary Table S1 is available at *Carcinogenesis* Online) from the 1814 bp amplicon and then was cloned into the pcDNA3.1 vector by XhoI and EcoRI.

Retrovirus production and cell transduction

HEK293T cells (3.5×10^6) were plated in 10 cm dishes and have a confluence of ∼70% after 20 h. Then, the cells were cotransfected with either 3.75 μg MSCVpuro-miR-26a or MSCVpuro vector, 3.75 μg gag-pol and 2.5 μg VSV-G using FuGENE 6. The supernatant containing the retrovirus was harvested at 48 h and filtered through a 0.45 μm low protein-binding-polysulfonic filter (Millipore, Bedford, MA). MCF7 cells, inoculated in advance in six-well plates and presenting with ∼50% confluence after 18 h, were infected with 3 ml filtered retrovirus suspension in the presence of 8 μg/ml polybrene (Chemicon, Temecula, CA). After transduction for 48 h, MCF7 cells were passaged into 10 cm dishes and allowed to grow for 12 h before transfectants were selected with 1.35 μg/ml puromycin in 2 days. The selected cells were utilized for tumorigenesis and anchorage-independent growth assay.

Anchorage-independent growth analysis

After selection with puromycin, MCF7 cells infected with MSCVpuro-miR-26a or MSCVpuro were trypsinized and suspended in complete medium plus 0.4% agar (Bio-Rad, Hercules, CA). The cell and agar mixture was seeded on a 0.6% agar base layer with complete medium at a density of 1×10^3 cells per well in six-well plates. After growth for 21 days, colonies containing >50 cells were counted.

Western blot

Cell or tissue lysates were fractionated by sodium dodecyl sulfate–polyacrylamide gel electrophoresis and then transferred to nitrocellulose membrane (Axygen, Union City, CA). Following blocking in phosphate-buffered saline containing 5% fat-free milk, the nitrocellulose membrane was incubated with primary antibodies against MTDH (40-6400; Invitrogen, Camarillo, CA), EZH2 (3147; Cell Signaling Technology, Beverly, MA), Caspase-8 (551242; BD Biosciences Pharmingen, San Diego, CA), Caspase-9 (9502; Cell Signaling Technology, Beverly, MA) or β-actin (CP01; Calbiochem, San Diego, CA) overnight at 4°C and then incubated with horseradish peroxidase-conjugated anti-mouse or rabbit IgG for 1 h at room temperature. The antigen–antibody immunoreactivity was detected in a sensitive digital imaging equipment (ImageQuant LAS 4000 mini; GE Healthcare Bio-Sciences AB, Uppsala, Sweden) using a commercial ECL detection kit (Millipore, Billerica, MA). The optical density of protein fragments was quantified by Quantity One software (Bio-Rad, Hercules, CA).

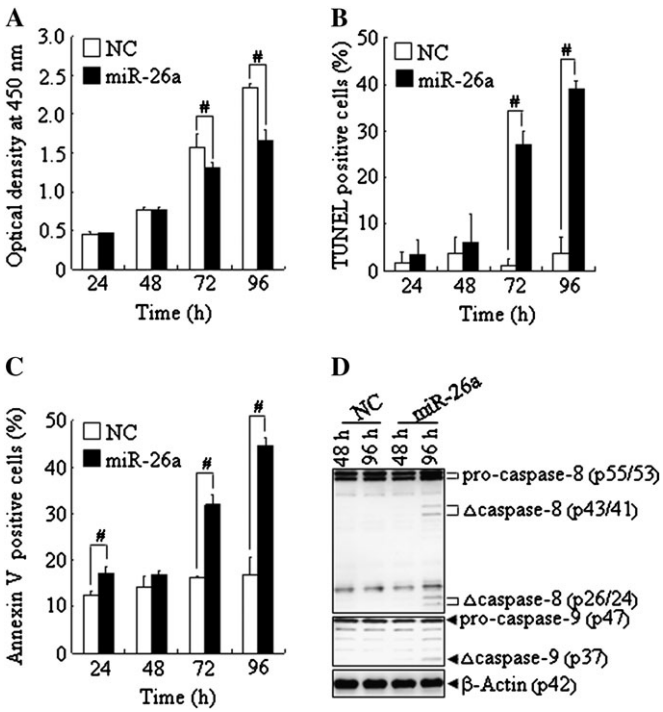

Fig. 2. miR-26a impairs viability and initiates apoptosis of MCF7 cells *in vitro*. (**A**) Viability reduction of MCF7 cells in response to miR-26a overexpression. The sensitive colorimetric assay was employed to evaluate cell viability at 24, 48, 72 and 96 h post transfection. (**B**) DNA fragmentation detection of apoptotic MCF7 cells by TUNEL assay. For miR-26a-overexpressed MCF7 cells, the percentage of TUNEL-positive cells persistently increased after 72 h. (**C**) Apoptosis evaluation by fluorescein isothiocyanate-annexin V/propidium iodide-double staining. Early and late apoptotic cells were combined as fluorescein isothiocyanate-annexin V-positive cells that were employed as the criterion to calculate the percentage of cell apoptosis. The symbol * denotes statistical difference ($P < 0.05$), whereas # represents great significant difference ($P < 0.01$) in a two-tailed Student's *t*-test for panels A–C. (**D**) Activation of caspase-8/9 due to miR-26a overexpression in MCF7 cells. 'Δ' means cleaved fragments. For MCF7 cells transfected with miR-26a at 96 h, pro-caspase-8 was cleaved to form four active fragments, p43, p41, p26 and p24, whereas only the autocleaved product p37 was visualized for pro-caspase-9. β-Actin was loaded as an internal control.

Downloaded from https://academic.oup.com/carcin/article/32/1/2/2477079 by U.S. Department of Justice user on 17 August 2022

Tumorigenesis assay in nude mice

Animal-related experiments were performed according to the Guide for the Care and Use of Laboratory Animals (National Institutes of Health Publications No. 80-23, revised 1996) and approved by the committee for humane treatment of animals at Shanghai Jiao Tong University School of Medicine. To assess whether miR-26a impacts tumorigenesis, ten 5-week-old BALB/c female nude mice were randomly divided into two equal groups. MCF7 cells (1.0×10^6), infected with either MSCVpuro-miR-26a or MSCVpuro, were suspended in 50 μl sterile 1× phosphate-buffered saline and orthotopically transplanted into the mammary fat pad using BD ultra-fine™ needle insulin syringe (BD Diabetes, Franklin Lakes, New Jersey). Both the long and short diameters of xenografts were measured using vernier calipers in on days 7, 11, 14, 17, 21, 25 and 30 and the corresponding tumor volume was calculated with the formula, volume = 1/6 [π × long diameter × (short diameter)^2]. At day 30, all mice were killed and tumors were isolated, entrapped with optimal cutting temperature (Sakura Finetek, Torrance, CA) in liquid nitrogen for 60 s and immediately reserved in −80°C for standard immunohistochemistry analysis.

Immunohistochemistry

Frozen section-based immunohistochemistry analysis was performed to detect MTDH and EZH2 expression in human MCF7 cell xenografts in nude mice. Briefly, optimal cutting temperature-entrapped specimens were sliced as 4 μm sections and dried for 1 h at room temperature. The sections were treated with 3% H_2O_2 in methanol for 10 min at room temperature to quench the endogenous peroxidase activity, followed by incubation with 1% bovine serum albumin for 1 h at 37°C to antagonize non-specific binding. Fifty microliters antibody of either mouse anti-human MTDH or rabbit anti-human EZH2, diluted at the respective ratios of 1:50 and 1:45, was incubated with the sections for 1 h at 37°C. After removal of the remaining antibody, the sections were further incubated with horseradish peroxidase-conjugated anti-mouse/rabbit IgG (KIT-5010; Maixin, Fujian, China) at room temperature for 15 min. The tissue sections were immersed in 3.3′-diaminobenzidine and the reaction was terminated when positive staining was present. Subsequently, hematoxylin was used to counterstain the sections for 10 min at room temperature. Following dehydration and mount, the sections were visualized. The brown or sepia staining signal denotes MTDH- or EZH2-positive regions.

Statistical analysis

Data are presented as mean ± standard error. Error bars indicate standard deviation. Generally, a two-tailed Student's *t*-test was employed to evaluate the differences between groups. Differences are considered as significant when the P value is <0.05.

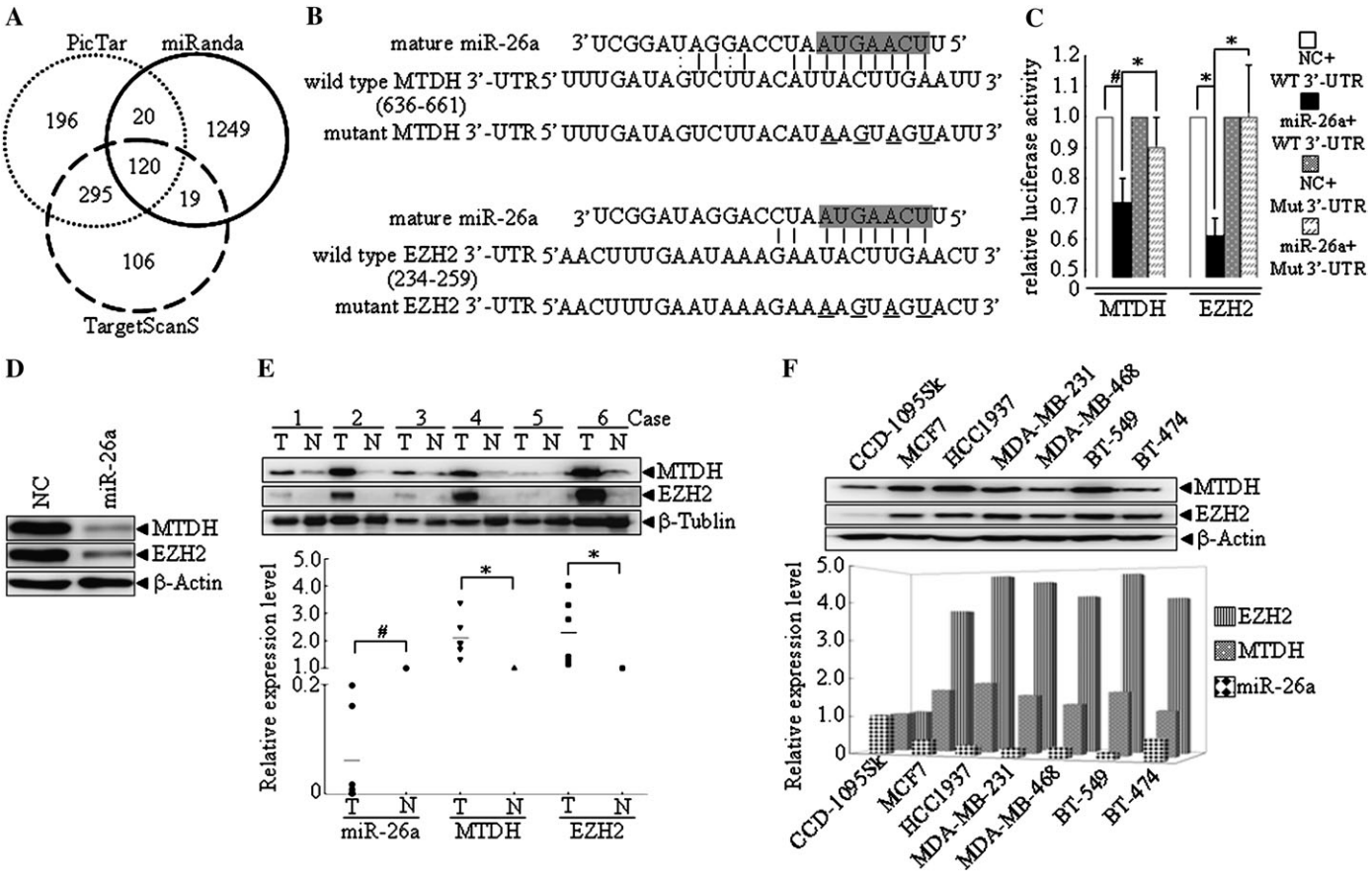

Fig. 3. MTDH and EZH2 are direct targets of miR-26a and are negatively correlated with miR-26a expression in breast cancer. (**A**) Venn diagram displaying numbers of computationally predicted miR-26a targets by three algorithms PicTar, miRanda and TargetScanS. (**B**) Putative miR-26a-binding sites in the 3′-UTRs of MTDH and EZH2. The miR-26a seed region is highlighted in gray. The numbers in the bracket denote the location of bases oriented from 5′ to 3′ in the 3′-UTR. The 4 bp mutation was generated in the 3′-UTRs of MTDH and EZH2 in the complementary sites with miR-26a and is underlined. (**C**) Relative activity of the luciferase gene fused with the wild-type or mutant 3′-UTRs of MTDH and EZH2 genes. The symbols * and # indicate significant ($P < 0.05$) and great significant difference ($P < 0.01$) following a two-tailed Student's *t*-test, respectively. (**D**) Decreased expression of endogenous MTDH and EZH2 due to miR-26a overexpression in MCF7 cells. β-Actin is shown as a loading control. (**E**) Expression and correlation of miR-26a and MTDH/EZH2 in paired clinical breast cancer samples. In the upper panel, N and T mean adjacent normal tissue and paired breast carcinoma, respectively. The expression level of MTDH/EZH2 was designated as the ratio of optical intensity between MTDH/EZH2 and β-tubulin in each lane, whereas the relative abundance of miR-26a was determined by stem-loop RT–PCR. For miR-26a and MTDH/EZH2, their expression level was assumed as 1 in adjacent normal tissues and corresponding calculated in paired tumor tissues. In lower panel, '−' indicates the mean of miR-26a or MTDH/EZH2 expression level. The significant difference ($^*P < 0.05$) and great significant difference ($\#P < 0.01$) were evaluated using paired-samples T test. (**F**) The expression level of miR-26a and MTDH/EZH2 in CCD-1095Sk and six breast cancer cell lines. The expression level of miR-26a and MTDH/EZH2 in CCD-1095Sk cells was considered as 1 while that of other six breast cancer cell lines was further determined by stem-loop RT–PCR and western blot, respectively. In lower panel, − indicates the mean of miR-26a or MTDH/EZH2 expression level. The inverse correlation between the miR-26a expression level and MTDH/EZH2 was shown in the lower panel.

Downloaded from https://academic.oup.com/carcin/article/32/1/2/2477079 by U.S. Department of Justice user on 17 August 2022

Results

Downregulation of miR-26a in breast cancer

To investigate the role of miR-26a in human breast tumorigenesis, we first compared the expression levels between clinical breast carcinomas and paired adjacent normal tissues. By stem-loop RT–PCR, we showed that the expression levels of miR-26a were reduced in 26 of 29 cases of breast tumor specimens ($P < 0.001$) compared with those of paired normal tissues (Figure 1A; supplementary Table S2 is available at *Carcinogenesis* Online). Furthermore, the HER2 status and age of breast cancer patients are significantly associated with the expression level of miR-26a (supplementary Table S3 is available at *Carcinogenesis* Online). We further evaluated the expression levels of miR-26a in six human breast cancer cell lines, MCF7, HCC1937, MDA-MB-231, MDA-MB-468, BT-549 and BT-474, as well as CCD-1095Sk. The expression levels of miR-26a were uniformly reduced in investigated breast cancer cell lines by 44.78–84.29% compared with that of CCD-1095Sk cells (Figure 1B). Thus, these results indicate that miR-26a is significantly downregulated in breast carcinoma.

MiR-26a impairs viability and initiates apoptosis of MCF7 cells

To define the function of clinically decreased miR-26a in the development of breast cancer, we transiently transfected MCF7 cells with NC or miR-26a mimics and evaluated cell viability by using a sensitive colorimetric assay. The viability of MCF7 cells transfected with the miR-26a mimic rather than NC was significantly decreased at 72 and 96 h (Figure 2A). Moreover, the morphologic observation showed that MCF7 cells transfected with miR-26a exhibited features characteristic of apoptosis, including blebbing, blurred edges, detachment from matrix and mass cell debris, which increased progressively after 72 h. Therefore, we tried to detect whether miR-26a overexpressed MCF7 cells undergo apoptosis. Indeed, MCF7 cells transfected with miR-26a mimic showed high percentage of TUNEL-positive cells, which reached to 27.02 and 39.10% at 72 and 96 h, respectively (Figure 2B; supplementary Figure S1 is available at *Carcinogenesis* Online). By annexin V/propidium iodide-double staining-based flow cytometry analysis, we further confirmed that the overexpression of miR-26a promoted spontaneous apoptosis of MCF7 cells from 17.3 to 44.5%, whereas cells transfected with NC did not produce noticeable changes from 48 to 96 h (Figure 2C; supplementary Figure S2 is available at *Carcinogenesis* Online).

Next, we assessed the expression level of apoptosis-related proteins by western blot. A time-course analysis of caspase-8 and caspase-9 was implemented for MCF7 cells transfected with NC or miR-26a mimics at 48 and 96 h, the two representative time points when cells recovered from the cytotoxicity of Lipofectamine 2000 and displayed distinct morphologic characteristics of apoptosis. The activated caspase-8 subunits, including p43, p41, p26 and p24 (Figure 2D), were clearly observed at 96 h in MCF7 cells transfected with miR-26a but not in control cells. The pro-caspase-9 was processed only by autocleavage in the apoptosome, yielding a relevant activated 37 kD band in miR-26a overexpressed cells at 96 h (Figure 2D), confirming that these cells indeed underwent apoptosis and activated a family of pro-caspases. In conclusion, the above results indicated that miR-26a initiated cell apoptosis through both extrinsic and intrinsic pathways with caspase-8 and caspase-9 activation, respectively.

MiR-26a directly regulates two apoptosis-related genes, MTDH and EZH2

To elucidate the molecular mechanism of miR-26a-mediated biological functions, we performed systematic *in silico* analyses to explore miR-26a targets. There are 120 genes simultaneously predicted as putative miR-26a targets by three programs, TargetScanS, PicTar and miRanda (Figure 3A). Combining the computationally predicted targets with the genes upregulated >2-fold from the gene expression profiles of 47 clinical breast tumor cases (17), we identified 8 potential miR-26a targets that were subjected to ranking by the miRanda algorithm. We chose the second best target, MTDH (supplementary Table S4 is available at *Carcinogenesis* Online), for in-depth investigation; interestingly, it was shown that MTDH may be responsible for the development of chemoresistance in breast cancer cells (23). Additionally, upregulated as high as 10.114-fold in breast cancer, EZH2 showed the greatest change among the predicted targets (supplementary Table S4 is available at *Carcinogenesis* Online). EZH2 was previously identified as a functional target of miR-26a in rhabdomyosarcoma and myc-induced lymphoma (8,14).

Based on the above analysis, we performed the luciferase reporter assay in HEK293 cells. As shown in microRNA:messenger RNA alignment analysis (Figure 3B), 652–658 nt and 250–256 nt, oriented from the 5′ end of 3′-UTR, were putative binding sites for miR-26a in 3′-UTR of MTDH and EZH2 genes, respectively. A truncated 3′-UTR of MTDH and a full-length 3′-UTR of EZH2, both of which contain miR-26a-binding sites, were cloned immediately downstream of the firefly luciferase gene in the pMIR-REPORT vector. HEK293 cells were transiently transfected with these constructs along with NC or miR-26a mimics. The miR-26a mimic, but not the NC, significantly suppressed the luciferase activity of reporter genes containing the 3′-UTRs of MTDH or EZH2. Moreover, 4 bp mutation in the 3′-UTR of MTDH and EZH2 genes corresponding to the position of 2, 4, 6 and 8 oriented from the 5′ terminus of mature miR-26a abolished the repression (Figure 3Band C). These results indicate that the effect of

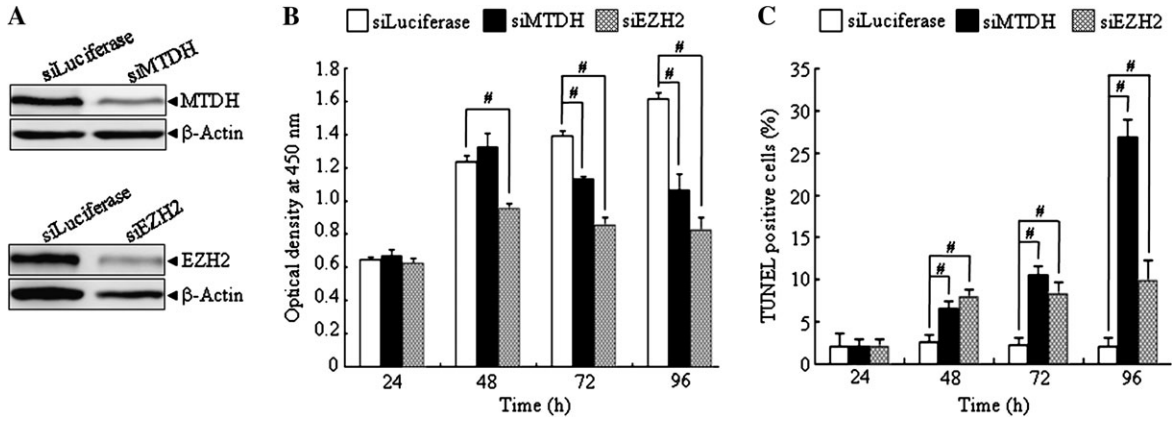

Fig. 4. MTDH and EZH2 knockdowns phenocopy miR-26a-mediated phenotype in MCF7 cells. (**A**) Detection of endogenous MTDH and EZH2 expression at 48 h after transfection of siMTDH or siEZH2 in MCF7 cells. β-Actin served as an internal control. (**B**) Viability evaluation of MCF7 cells at 24, 48, 72 and 96 h post transfection of siMTDH or siEZH2. (**C**) TUNEL assay of MCF7 cells transfected with siMTDH or siEZH2. The TUNEL-positive cells are present at 48 h post siMTDH or siEZH2 transfection. The symbol * denotes statistical difference ($P < 0.05$), whereas # represents great significant difference ($P < 0.01$) in a two-tailed Student's *t*-test.

Downloaded from https://academic.oup.com/carcin/article/32/1/2/2477079 by U.S. Department of Justice user on 17 August 2022

miR-26a is due to specific and direct interaction with the putative binding sites in the 3′-UTRs of MTDH and EZH2.

To further investigate whether miR-26a expression affects the expression level of MTDH and EZH2, MCF7 cells were transiently transfected with NC or miR-26a mimics. Compared with NC, overexpression of miR-26a efficiently inhibited endogenous expression of both MTDH and EZH2 at 72 h after transfection (Figure 3D). Moreover, there is a similar inverse correlation between the expression level of miR-26a and MTDH/EZH2 in clinical samples and breast cancer cell lines (Figure 3E and F). Together, the above results demonstrate that miR-26a suppresses the expression of both MTDH and EZH2 by directly targeting their 3′-UTR.

MTDH and EZH2 are involved in miR-26a-induced apoptosis

To investigate whether miR-26a-induced apoptosis is ascribable to their targets, we first silenced MTDH and EZH2 expression to phenocopy the miR-26a-mediatied phenotype. MCF7 cells were transfected with siLuciferase, siMTDH or siEZH2 and the optical density values were detected at 24, 48, 72 and 96 h. SiMTDH and siEZH2 efficiently silenced MTDH and EZH2 gene expression, respectively (Figure 4A). Knockdown of MTDH in MCF7 cells attenuated cell viability after 72 h, whereas silencing of EZH2 significantly decreased cell viability after 48 h (Figure 4B). Moreover, the cell viability impairment is progressively enhanced, which was similar to the miR-26a-induced viability impairment in MCF7 cells (Figure 4B). On the other hand, the TUNEL-positive MCF7 cells appeared at 48 h after transfection of siMTDH or siEZH2 and are significantly increased in cells transfected with siMTDH rather than siEZH2 (Figure 4C; supplementary Figure S3 is available at *Carcinogenesis* Online).

Next, we examined whether the restoration of miR-26a target MTDH can reverse the miR-26a-mediated apoptosis. After transfection of NC or miR-26a mimics in MCF7 cells for 24 h, we further transfected pcDNA3.1-MTDH or control plasmids. Transfection of pcDNA3.1-MTDH efficiently restored MTDH expression in MCF7 cells with enhanced expression of miR-26a (Figure 5A). As expected, in the miR-26a-transfected MCF7 cells, reexpression of MTDH abrogated cell viability impairment at 96 h and partially reversed cell apoptosis at 72 and 96 h, whereas the pcDNA3.1 empty vector failed to rescue miR-26a-mediated phenotype (Figure 5B and C; supplementary Figure S4 is available at *Carcinogenesis* Online). Therefore, MTDH is a functional target of miR-26a for its antitumorigenic role in MCF7 cells.

MiR-26a suppresses anchorage-independent growth in vitro and tumorigenesis in vivo

The observation that the miR-26a expression level was significantly decreased in breast tumor inspired us to investigate the functional role of miR-26a in tumorigenesis. First, anchorage-independent growth assay was evaluated in MCF7 cells infected with MSCVpuro or MSCVpuro-miR-26a. Consequently, miR-26a was overexpressed (supplementary Figure S5 is available at *Carcinogenesis* Online) and significantly delayed the colony formation ability of MCF7 cells as exhibited by the decreases in colony number and size ($P < 0.05$) (Figure 6A). These results implied that miR-26a might suppress tumorigenesis *in vivo*.

To further investigate the relationship between miR-26a and tumorigenesis *in vivo*, an orthotopic transplantation model of human breast carcinoma in nude mice was employed. Retrovirus-infected MCF7 cells were orthotopically inoculated into the mammary fat pad of female BALB/c nude mice. Tumor volume was monitored twice weekly during a 1 month period. Compared with the control group, the tumor volume from miR-26a transfectants was significantly reduced by Day 17 ($P < 0.05$) and was decreased further by 56.45% by Day 30 (Figure 6B and C). To reveal the molecular mechanism of tumor suppression mediated by miR-26a, all mice were killed at 30 days and the tumors were prepared as frozen sections for further analysis. The TUNEL assay showed that the miR-26a-overexpressed MCF7 xenografts contained more apoptotic cells (12.71%) than that of the control cells (4.14%) (Figure 6D). Moreover, the tumors derived from the miR-26a-overexpressed MCF7 cells showed a decrease in the expression of MTDH and EZH2 through a standard immunohistochemistry approach (Figure 6E). These results suggest that miR-26a can suppress tumorigenesis of human MCF7 xenocrafts by inducing cell apoptosis in nude mice, which is at least partly attributed to the decreased expression of MTDH and EZH2.

Discussion

MicroRNAs play important regulatory roles in the development and progression of various cancers (2,30). Here, we report that miR-26a is pathologically downregulated in human breast cancers. Apoptosis mediated by miR-26a is partly attributed to its regulation of MTDH and EZH2. Moreover, miR-26a suppresses tumorigenesis of MCF7

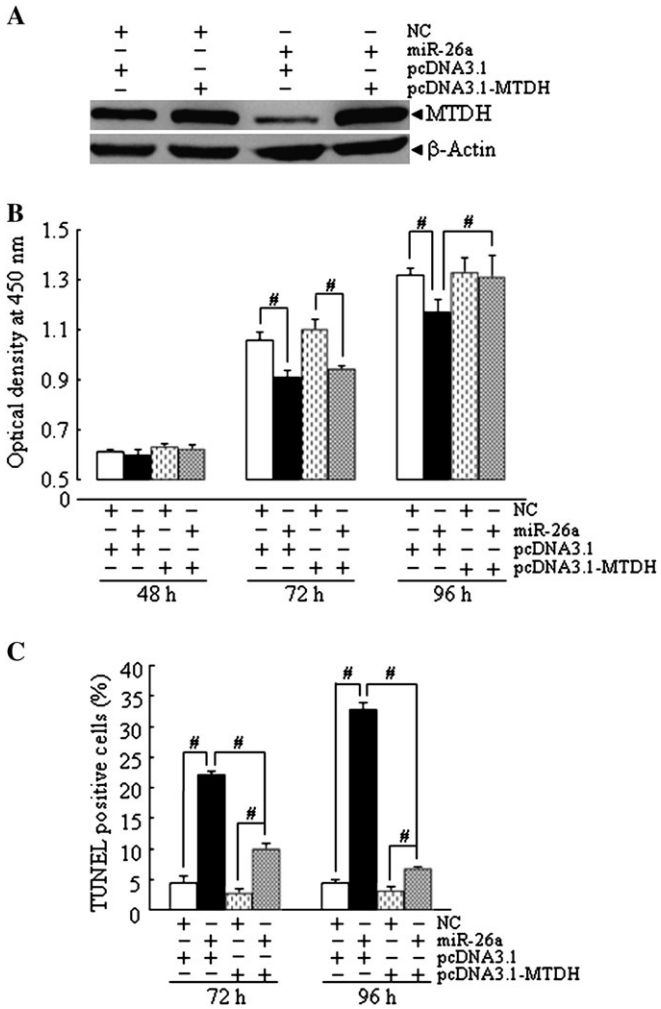

Fig. 5. MTDH can partially reverse miR-26a-induced apoptosis in MCF7 cells. (**A**) Expression of pcDNA3.1-MTDH in MCF7 cells transfected with NC or miR-26a mimics. β-Actin is shown as a loading control. (**B**) Viability evaluation of MCF7 cells transfected with NC or miR-26a mimics together with either pcDNA3.1-MTDH or control vector. Following transfection of 100 nM NC or miR-26a mimics for 24 h, MCF7 cells were further transfected with 100 ng pcDNA3.1-MTDH or control vector and allowed to grow for another three days. The optical values at 450 nm were measured at 48, 72 and 96 h. (**C**) TUNEL assay of MCF7 cells transfected with NC or miR-26a mimics together with either pcDNA3.1-MTDH or control vector. The proportion of apoptotic cells due to distinct treatment is shown in the *y*-axis. The symbol * denotes statistical difference ($P < 0.05$), whereas # represents great significant difference ($P < 0.01$) in a two-tailed Student's *t*-test.

Downloaded from https://academic.oup.com/carcin/article/32/1/2/2477079 by U.S. Department of Justice user on 17 August 2022

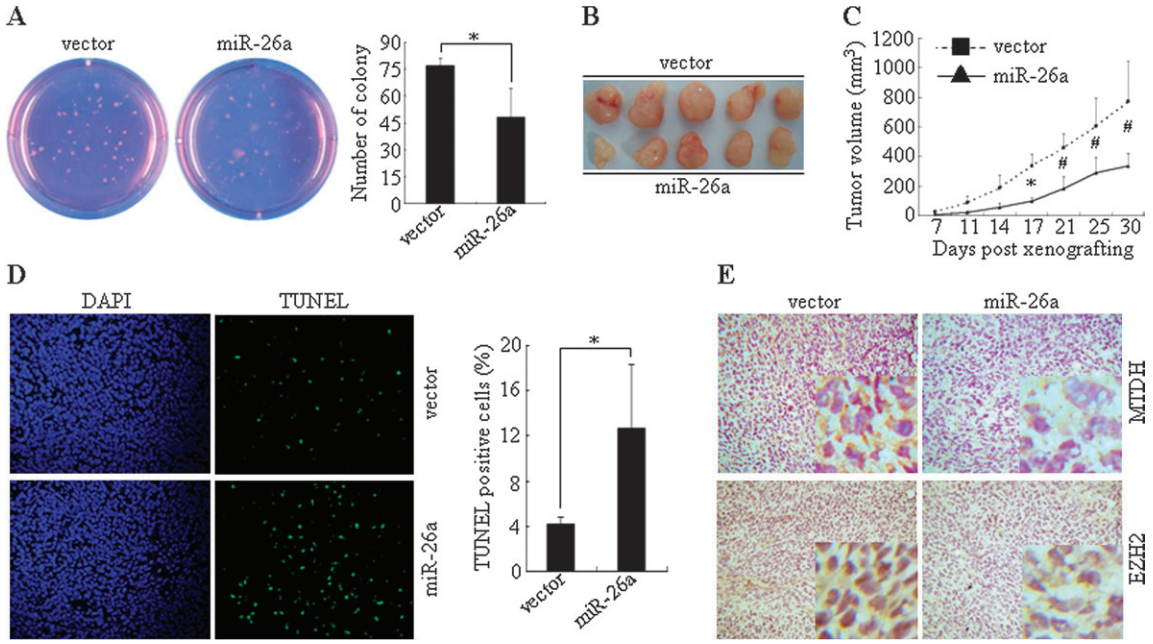

Fig. 6. Effect of miR-26a on colony formation and tumorigenesis of MCF7 cells. (**A**) Influence of miR-26a on colony formation of MCF7 cells. Representative dishes are presented (left panel). The number of clones was counted for each well of six-well plates and shown in the *y*-axis of the right panel. (**B**) Effect of miR-26a on tumorigenesis in an orthotopic xenograft mouse model. After 1 month, all mice orthotopically transplanted with retrovirus-infected MCF7 cells were killed and tumors were separated. (**C**) Growth curve of MCF7 cell engrafted tumors in nude mice. The tumor dimensions were measured every 3 or 4 days and their volumes were calculated and plotted as mean ± standard derivation from five mice of each category. (**D**) TUNEL assay in xenografts. For vector or miR-26a-involved tumor specimens, 4,6-diamidino-2-phenylindole and TUNEL-double staining was processed in each frozen section. Representative fields were chosen and presented (left panel). The percentage of TUNEL-positive cells is shown in the *y*-axis (right panel). The two-tailed Student's *t*-test was employed to test the difference of colony number (A), tumor volume (C) and TUNEL-positive rate (D) for retrovirus-infected MCF7 cells or their xenografts. The symbols * and # are regarded as significant and great significant differences with $P < 0.05$ and $P < 0.01$, respectively. (**E**) Immunohistochemistry analysis of MTDH and EZH2 expression for tumor sections. Immunohistochemical staining shows that EZH2 is located in the nucleus, whereas MTDH has a diffuse distribution but is mainly accumulated in membrane-related structures in cancer cells of MCF7 xenografts. The pictures with a magnification of ×5 are further shown in the right bottom of each panel. Tumor specimens from MCF7 cells with empty vector infection show higher expression level of EZH2 and especially MTDH than that of MSCVpuro-miR-26a-infected MCF7 cell engraftments.

xenografts in an orthotopical transplantation mouse model. In conclusion, our studies show that miR-26a functions as a tumor suppressor in human breast cancer.

The decreased expression of miR-26a in breast carcinomas may result from multiple regulatory events, including loss of heterozygosity at chromosome 3p22, transcription regulators mutation such as p53 and the expression level of Dicer (10,31–33). Similarly, both MTDH and EZH2 also undergo complicated regulation in breast carcinomas. The MTDH gene is located at chromosome region 8q22, a frequently amplified region in clinical breast cancers. The gain of 8q22 DNA copy number contributes to the increased protein level of MTDH. However, 12% of clinical breast cancer samples with normal 8q22 DNA copy number showed high protein level of MTDH (23). Similarly, amplification of EZH2 locus 7q36 was observed in 15% of breast cancers but the cause of the high expression level was not deciphered (34). Theoretically, downregulation of miR-26a should contribute to the increased expression of MTDH and EZH2 in breast cancers as an alterative mechanism.

To date, experimentally validated miR-26a targets contain eight genes, SMAD family member 1 (SMAD1) (35), EZH2 (8), interleukin 6 (IL-6) (36), CCND2 (7), CCNE2 (7), PTEN (6,8), RB1 (6) and MAP3K2 (6). In this study, we identify MTDH as a new functional target of miR-26a and EZH2 as a miR-26a target in breast cancer.

Our observations imply that the loss of miR-26a may result in gained expression of MTDH and EZH2, which endows tumor cells with the ability to develop chemoresistance and in turn favors tumor progression. Moreover, miR-26a could probably contribute to key apoptotic pathways as a downstream effector, such as in the p53-induced apoptosis (31,37). The breast tumorigenesis is a micro-evolutionary process involving the evasion of apoptosis from the host surveillance system. We may reasonably speculate that the restoration of miR-26a activity may represent an attractive strategy for breast cancer therapy. In addition, high expression of miR-26a is detected in a wide variety of human normal tissues (7), which endows the human body with the advantage to tolerate the therapeutic dose delivery in normal tissues. Of significance, systemic administration of miR-26a delivery using adeno-associated virus (16) strikingly antagonized tumorigenesis without toxicity in a mouse model of MYC-induce liver cancer (7). Given the potent effect of miR-26a on tumor cell apoptosis in this study, future studies are expected to manipulate miR-26a as a clinically viable anticancer agent to achieve therapy of breast cancer and even other cancers.

Supplementary material

Supplementary Figures 1–5 and Table S1–S4 can be found at http://carcin.oxfordjournals.org/

Funding

National Key Program (973) for Basic Research of China (2009CB918404); National High-tech R&D Program (2008AA02Z301); National Science Foundation of China (90813034, 30630034 and 30870979); Science and Technology Committee of Shanghai (08JC1413700, 08JC1413500); 'Shu Guang' project supported by Shanghai Municipal Education Commission and Shanghai Education Development Foundation (09SG18 to Shu Guang).

Downloaded from https://academic.oup.com/carcin/article/32/1/2/2477079 by U.S. Department of Justice user on 17 August 2022

Acknowledgements

The Genminix company provides us with technical assistance. We extend our thanks to Professor Jian-Xiu Yu and Professor Han-Yi Zhuang for modification of the manuscript.

Conflict of Interest Statement: None declared.

References

1. Bartel,D.P. (2004) MicroRNAs: genomics, biogenesis, mechanism, and function. *Cell*, **116**, 281–297.
2. Chen,C.Z. (2005) MicroRNAs as oncogenes and tumor suppressors. *N. Engl. J. Med.*, **353**, 1768–1771.
3. Calin,G.A. *et al*. (2004) Human microRNA genes are frequently located at fragile sites and genomic regions involved in cancers. *Proc. Natl Acad. Sci. USA*, **101**, 2999–3004.
4. Calin,G.A. *et al*. (2006) MicroRNA signatures in human cancers. *Nat. Rev. Cancer*, **6**, 857–866.
5. Iorio,M.V. *et al*. (2005) MicroRNA gene expression deregulation in human breast cancer. *Cancer Res.*, **65**, 7065–7070.
6. Kim,H. *et al*. (2010) Integrative genome analysis reveals an oncomir/oncogene cluster regulating glioblastoma survivorship. *Proc. Natl Acad. Sci. USA*, **107**, 2183–2188.
7. Kota,J. *et al*. (2009) Therapeutic microRNA delivery suppresses tumorigenesis in a murine liver cancer model. *Cell*, **137**, 1005–1017.
8. Sander,S. *et al*. (2008) MYC stimulates EZH2 expression by repression of its negative regulator miR-26a. *Blood*, **112**, 4202–4212.
9. Zhang,L. *et al*. (2006) microRNAs exhibit high frequency genomic alterations in human cancer. *Proc. Natl Acad. Sci. USA*, **103**, 9136–9141.
10. Chen,L.C. *et al*. (1994) Deletion of two separate regions on chromosome 3p in breast cancers. *Cancer Res.*, **54**, 3021–3024.
11. Dahiya,R. *et al*. (1997) Chromosome 3p24-26 and 3p22-12 loss in human prostatic adenocarcinoma. *Int. J. Cancer*, **71**, 20–25.
12. Huse,J.T. *et al*. (2009) The PTEN-regulating microRNA miR-26a is amplified in high-grade glioma and facilitates gliomagenesis *in vivo*. *Genes Dev.*, **23**, 1327–1337.
13. Ji,J. *et al*. (2009) MicroRNA expression, survival, and response to interferon in liver cancer. *N. Engl. J. Med.*, **361**, 1437–1447.
14. Ciarapica,R. *et al*. (2009) Deregulated expression of miR-26a and Ezh2 in rhabdomyosarcoma. *Cell Cycle*, **8**, 172–175.
15. Maillot,G. *et al*. (2009) Widespread estrogen-dependent repression of micrornas involved in breast tumor cell growth. *Cancer Res.*, **69**, 8332–8340.
16. Lu,J. *et al*. (2005) MicroRNA expression profiles classify human cancers. *Nature*, **435**, 834–838.
17. Richardson,A.L. *et al*. (2006) X chromosomal abnormalities in basal-like human breast cancer. *Cancer Cell*, **9**, 121–132.
18. Emdad,L. *et al*. (2009) Astrocyte elevated gene-1 (AEG-1) functions as an oncogene and regulates angiogenesis. *Proc. Natl Acad. Sci. USA*, **106**, 21300–21305.
19. Kleer,C.G. *et al*. (2003) EZH2 is a marker of aggressive breast cancer and promotes neoplastic transformation of breast epithelial cells. *Proc. Natl Acad. Sci. USA*, **100**, 11606–11611.
20. Li,J. *et al*. (2008) Astrocyte elevated gene-1 is a novel prognostic marker for breast cancer progression and overall patient survival. *Clin. Cancer Res.*, **14**, 3319–3326.
21. Kikuno,N. *et al*. (2007) Knockdown of astrocyte-elevated gene-1 inhibits prostate cancer progression through upregulation of FOXO3a activity. *Oncogene*, **26**, 7647–7655.
22. Liu,H. *et al*. (2009) Knockdown of astrocyte elevated gene-1 inhibits proliferation and enhancing chemo-sensitivity to cisplatin or doxorubicin in neuroblastoma cells. *J. Exp. Clin. Cancer Res.*, **28**, 19.
23. Hu,G. *et al*. (2009) MTDH activation by 8q22 genomic gain promotes chemoresistance and metastasis of poor-prognosis breast cancer. *Cancer Cell*, **15**, 9–20.
24. Lee,S.G. *et al*. (2006) Astrocyte elevated gene-1 (AEG-1) is a target gene of oncogenic Ha-ras requiring phosphatidylinositol 3-kinase and c-Myc. *Proc. Natl Acad. Sci. USA*, **103**, 17390–17395.
25. Shi,B. *et al*. (2007) Integration of estrogen and Wnt signaling circuits by the polycomb group protein EZH2 in breast cancer cells. *Mol. Cell. Biol.*, **27**, 5105–5119.
26. Schuettengruber,B. *et al*. (2007) Genome regulation by polycomb and trithorax proteins. *Cell*, **128**, 735–745.
27. Bracken,A.P. *et al*. (2007) The Polycomb group proteins bind throughout the INK4A-ARF locus and are disassociated in senescent cells. *Genes Dev.*, **21**, 525–530.
28. Wagener,N. *et al*. (2008) The enhancer of zeste homolog 2 gene contributes to cell proliferation and apoptosis resistance in renal cell carcinoma cells. *Int. J. Cancer*, **123**, 1545–1550.
29. Chen,C. *et al*. (2005) Real-time quantification of microRNAs by stem-loop RT-PCR. *Nucleic Acids Res.*, **33**, e179.
30. Yu,F. *et al*. (2007) let-7 regulates self renewal and tumorigenicity of breast cancer cells. *Cell*, **131**, 1109–1123.
31. Suzuki,H.I. *et al*. (2009) Modulation of microRNA processing by p53. *Nature*, **460**, 529–533.
32. Mazars,R. *et al*. (1992) p53 mutations occur in aggressive breast cancer. *Cancer Res.*, **52**, 3918–3923.
33. Grelier,G. *et al*. (2009) Prognostic value of Dicer expression in human breast cancers and association with the mesenchymal phenotype. *Br. J. Cancer*, **101**, 673–683.
34. Bracken,A.P. *et al*. (2003) EZH2 is downstream of the pRB-E2F pathway, essential for proliferation and amplified in cancer. *EMBO J.*, **22**, 5323–5335.
35. Luzi,E. *et al*. (2008) Osteogenic differentiation of human adipose tissue-derived stem cells is modulated by the miR-26a targeting of the SMAD1 transcription factor. *J. Bone Miner. Res.*, **23**, 287–295.
36. Jones,M.R. *et al*. (2009) Zcchc11-dependent uridylation of microRNA directs cytokine expression. *Nat. Cell Biol.*, **11**, 1157–1163.
37. Yu,J. *et al*. (2007) A network of p73, p53 and Egr1 is required for efficient apoptosis in tumor cells. *Cell Death Differ.*, **14**, 436–446.

Received August 10, 2010; revised September 28, 2010; accepted October 6, 2010

Downloaded from https://academic.oup.com/carcin/article/32/1/2/2477079 by U.S. Department of Justice user on 17 August 2022